First online multireflection time-of-flight mass measurements of isobar chains produced by fusion-evaporation reactions: Toward identification of superheavy elements via mass spectroscopy

doi: 10.1103/PhysRevC.95.011305

PHYSICAL REVIEW C **95**, 011305(R) (2017)

First online multireflection time-of-flight mass measurements of isobar chains produced by fusion-evaporation reactions: Toward identification of superheavy elements via mass spectroscopy

P. Schury,[1,2,3] M. Wada,[1,2] Y. Ito,[2] D. Kaji,[2] F. Arai,[2] M. MacCormick,[4] I. Murray,[4] H. Haba,[2] S. Jeong,[1] S. Kimura,[1,2,3] H. Koura,[5] H. Miyatake,[1] K. Morimoto,[2] K. Morita,[2,6] A. Ozawa,[3] M. Rosenbusch,[2] M. Reponen,[2] P.-A. Söderström,[2] A. Takamine,[2] T. Tanaka,[2,6] and H. Wollnik[7]

[1]*Wako Nuclear Science Center (WNSC), Institute of Nuclear and Particle Science (IPNS), High Energy Accelerator Research Organization (KEK), Wako, Saitama 351-0198, Japan*

[2]*RIKEN Nishina Center for Accelerator-Based Science, Wako, Saitama 351-0198, Japan*

[3]*Institute of Physics, University of Tsukuba, Ibaraki 305-8571, Japan*

[4]*Institut de Physique Nucléaire, IN2P3-CNRS, Université Paris-Sud, Université Paris-Saclay, 91406 Orsay Cedex, France*

[5]*Advanced Science Research Center, Japan Atomic Energy Agency, Ibaraki 319-1195, Japan*

[6]*Kyushu University, Hakozaki, Higashi-ku, Fukuoka 812-8581, Japan*

[7]*New Mexico State University, Las Cruces, New Mexico 88001, USA*

(Received 27 October 2015; revised manuscript received 2 October 2016; published 30 January 2017)

Using a multireflection time-of-flight mass spectrograph located after a gas cell coupled with the gas-filled recoil ion separator GARIS-II, the masses of several α-decaying heavy nuclei were directly and precisely measured. The nuclei were produced via fusion-evaporation reactions and separated from projectilelike and targetlike particles using GARIS-II before being stopped in a helium-filled gas cell. Time-of-flight spectra for three isobar chains, ^{204}Fr-^{204}Rn-^{204}At-^{204}Po, ^{205}Fr-^{205}Rn-^{205}At-^{205}Po-^{205}Bi, and ^{206}Fr-^{206}Rn-^{206}At, were observed. Precision atomic mass values were determined for $^{204–206}$Fr, ^{204,205}Rn, and ^{204,205}At. Identifications of ^{205}Bi, ^{204,205}Po, ^{206}Rn, and ^{206}At were made with $N \lesssim 10$ detected ions, representing the next step toward use of mass spectrometry to identify exceedingly low-yield species such as superheavy element ions.

DOI: 10.1103/PhysRevC.95.011305

In the search for the long-predicted "island of stability" [1], the use of so-called hot-fusion reactions has allowed for extending the observed periodic table of elements up to element 118 in recent years. However, a dearth of projectile-target combinations available for cross-bombardment reactions along with α-decay chains terminating in spontaneous fission before reaching well-known nuclei bottlenecked the International Union of Pure and Applied Chemistry's acceptance of elements 113, 115, 117, and 118 [2] until very recently. As we push ever closer to the island of stability, whether by use of more exotic projectile-target combinations or use of multinucleon transfer reactions [3], this problem will become ever more severe; we can expect many spontaneously fissioning nuclei, longer α-decay half-lives, and a recurrence of β-decay [4].

At present, such superheavy nuclei are identified via decay spectroscopy. To accomplish this, a position sensitive detector records implantations and decays; a gas-filled [5,6] or vacuum [7] separator limits the range of incoming ions to those with rigidity or velocity similar to the desired isotope. Chains of α-decays can then be correlated to detector implantation events to determine the identity of the incoming ions. However, this technique relies on the two-body nature of α-decay to provide precise decay energies used to "fingerprint" the decay. If spontaneous fission or β-decay becomes predominant, such decay spectroscopy will no longer be possible. Beyond that, reliable identification based on $N \ll 10$ events requires reasonably short half-lives of these nuclei to avoid background noise (e.g., cosmic rays, natural background radiation, etc.) from becoming a likelihood between implantation and initial decay or between subsequent decays. Were half-lives to extend to days, this would also make decay spectroscopy untenable.

In recent years multireflection time-of-flight mass spectrographs (MRTOF-MSs) [8], first proposed by Wollnik and Przewloka [9] more than 20 years ago, have begun to make an impact in nuclear physics as isobar separators [10,11], for use in precision mass measurements [12–14], and even in half-life measurements [15]. The MRTOF-MS could provide a means to change from a paradigm of identifying transactinide isotopes by α-decay chain to one of identification by mass determination.

The MRTOF-MS employs a pair of coaxial electrostatic mirrors, between which ions reflect back and forth, thus extending the flight path of ions. The electric potentials within the mirrors are carefully chosen to provide isochronous operation, wherein the depth that an ion penetrates into the mirror is related to the ion's energy such that after leaving the mirror all ions of a given species pass a specific location (a so-called time focus) at the same time without regard to their energy. By momentarily lowering the outermost potential on either mirror, ions can be allowed to enter or exit the MRTOF-MS. A detailed description can be found in Ref. [16].

The MRTOF-MS is well suited for low-yield, heavy, and short-lived nuclei. It achieves mass resolving powers $R_m >$ 100 000 with flight times shorter than 20 ms for even the heaviest nuclei [11,16]. Additionally, it is a true spectrograph—as opposed to a spectrometer—making it capable of mass determinations with, in principle, as few as one detected ion. Owing to its spectrographic nature, the MRTOF-MS is able to simultaneously measure several species with high precision. This capability has until now been limited to storage rings. As we have demonstrated [13,16], and herein further demonstrate, the MRTOF-MS allows for a considerably less complex data analysis than that used for storage rings.

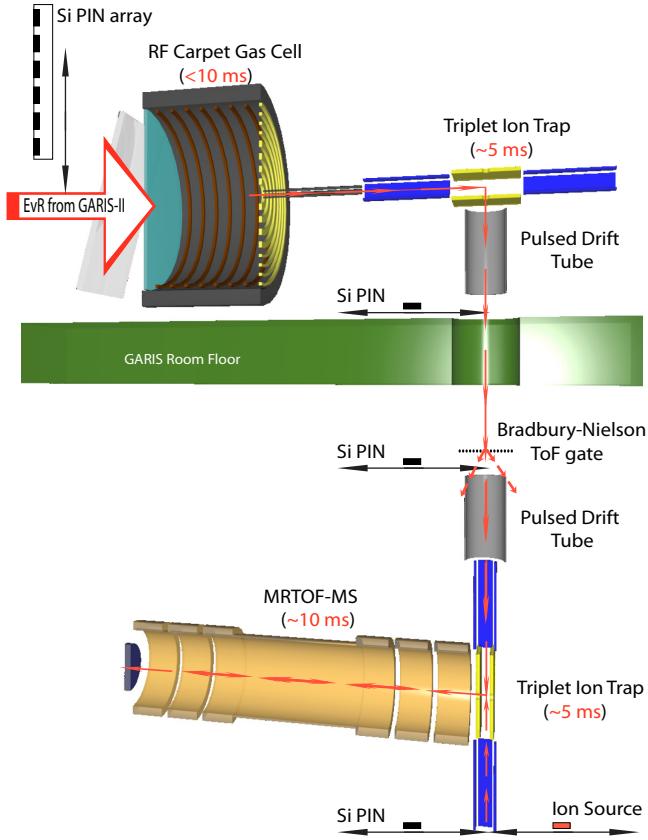

FIG. 1. Schematic overview of the experimental setup. Red arrows show the path of ions through the system. Red lettering gives time scale.

As the first step toward mass spectrographic identification of superheavy elements (SHEs), a gas cell connected to an MRTOF-MS was installed in front of the gas-filled recoil ion separator GARIS-II [6]. This system has been used to perform initial mass measurements of fusion-evaporation reaction products lighter than uranium, some of which have not previously been directly measured. In these measurements we demonstrate the ability of the MRTOF-MS to simultaneously measure the masses of atomic (and molecular) ions across multiple isobar chains. With high statistics a precision of $\delta m/m < 5 \times 10^{-7}$ can be achieved, while with fewer than 10 detected ions the mass can be determined with sufficient precision to identify an ion species. A brief description of the system is given here (see Fig. 1); however, a detailed description is published elsewhere [17].

A beam of ^{40}Ar was provided by the RIKEN heavy-ion linear accelerator RILAC. The beam impinged upon a rotating target wheel with 16 target windows. The target wheel comprised 4 windows of $^{165}_{67}$Ho with a thickness of $\sim$0.14 mg/cm^2 and 12 windows of $^{169}_{69}$Tm with a thickness of $\sim$0.29 mg/cm^2. The ^{165}Ho and ^{169}Tm targets were prepared using sputtering and electrodeposition methods, respectively, on 3 μm Ti backing foil. A rotating shadow wheel ensured the beam could only impinge on one type of target at a time [18].

When the projectile beam interacts with the target, the projectile and target nuclei can fuse to form a compound nucleus in an excited state. The compound nucleus will then rapidly deexcite by particle emission: typically multiple neutrons (xn), a proton and multiple neutrons (pxn), or an α particle and multiple neutrons (αxn) are emitted. The remaining evaporation products, in this case, will exit the target with an energy of $\sim$30 MeV and an energy spread of several percent.

The products were separated in flight from projectiles and targetlike particles using GARIS-II. The separator was filled with helium gas at 73 Pa. The ions passed through an exit window of 0.5-μm-thick Mylar upon leaving GARIS-II.

In order for these radioactive ions (RIs) to be captured in an ion trap, they were first stopped and thermalized in a helium-filled gas cell installed in the focal plane chamber following GARIS-II. A degrader was placed between the GARIS-II exit window and the gas cell's 2.5-μm-thick Mylar entrance window. This degrader consisted of a 4-μm-thick Mylar foil which could be rotated up to 45° to adjust the effective thickness. The gas cell was pressurized to $\approx$10 kPa.

A flat array of silicon PIN diodes could be inserted between the GARIS-II exit window and the rotatable degrader. From the α-decay spectrum we could identity and determine the rates of incoming ions. Using this insertable detector further allowed for the optimization of the magnetic rigidity setting of GARIS-II.

Ions were quickly extracted from the gas cell by use of an axial dc gradient and a circular traveling wave rf carpet [19]. The carpet is 8 cm in diameter with 80-μm wires and 80 μm spacing between wires and has a 320-μm-diam exit orifice, which provides an excellent differential pumping barrier. As ions left the gas cell via the small exit orifice, they were transported via rf-multipole ion guides to a triplet of rf quadrupole ion traps, similar to that reported in Ref. [20], where they accumulated and cooled. The ions were then orthogonally ejected from the central trap, accelerated by a pulsed drift tube to 1.5 keV, and transported 2.5 m to a second pulsed drift tube and deceleration optics, followed by a second set of rf-quadrupole traps wherein the ions were recaptured. Just prior to the second pulsed drift tube was a Bradbury-Nielson gate [21] capable of suppressing ions differing in A/q from the desired species with mass resolving power $R_{\rm m} \sim 100$. The central trap in the second trap triplet served as the final MRTOF preparation trap. After cooling in the final trap, ions were again orthogonally ejected and entered the MRTOF-MS, wherein they underwent a predetermined number of reflections before being released to a multichannel plate (MCP) detector. The ejection from the final trap served as a start signal for a time-to-digital converter (TDC) [22], while the signal on the MCP served as the TDC stop signal. The absolute time of flight for each detected ion was recorded with a precision of 100 ps, along with the cycle number. From accumulation in the first trap to detection at the MCP, the cycle was 30 ms.

Two measurement runs were performed focusing on ^{169}Tm(^{40}Ar, xn)$^{209-x}$Fr reaction products. In the first, a 1.5 pμA beam of ^{40}Ar^{11+} at 4.825 MeV/nucleon was employed to maximize $n = 3,4$ channels. In the second, a 0.8 pμA beam of ^{40}Ar^{11+} at 5.16 MeV/nucleon was employed to maximize $n = 4,5$ channels. Different MRTOF-MS settings were used in the two runs.

In the first measurement run, the MRTOF-MS was tuned such that it achieved a maximum mass resolving power of $R_m \approx 150\,000$ at $n = 148$ laps, giving a mass bandwidth [23] of 1.34%. In the second measurement run, the MRTOF-MS was tuned to provide $R_m \approx 120\,000$ at $n = 224$ laps, giving a mass bandwidth of 0.89%. Because of the limited mass bandwidth, ions differing in m/q from the species of interest by more than the mass bandwidth appear in the TOF spectrum having made a different number of laps than the ions of interest and could by chance coincide in TOF near the ions of interest. To avoid mistaken identifications, multiple measurements were performed using different numbers of laps; peaks that do not appear in every spectrum may represent contaminants making a different number of laps than the ions of interest.

We made use of a concomitant referencing method [24], to be described in detail in a subsequent publication, wherein online measurements and reference measurements are made sequentially in each cycle. The multitrap system allows one species to accumulate while the other is being analyzed, making the duty cycle ≈100% for concomitant referencing.

Each data run was of a duration longer than 30 min, allowing the spectral peaks to drift due to thermal expansion of the reflection chamber and high-voltage power supply instabilities on the level of parts per million [16]. In the concomitant referencing method, reference and online measurements drift together, allowing correction for such drifting. The data were divided into i subsets of equal duration such that in each subset the drift reference spectral peak fit had a relative precision of $\delta t/t < 2 \times 10^{-7}$. The time of flight for each ion was then adjusted according to

$$T = T_{\text{uncorrected}} t_i^{\text{ref}} / t_{i=0}^{\text{ref}}, \tag{1}$$

where T and $T_{\text{uncorrected}}$ represent the time of flight of an individual ion. The values T for all ions are then used to build a histogram representing the TOF spectrum.

Atomic masses were calculated from reference measurements in a single-reference analysis as described in Ref. [13]. The masses were determined using

$$m = \rho m_{\text{ref}} = \left(\frac{t - t_0}{t_{\text{ref}} - t_0} \right)^2 m_{\text{ref}}, \tag{2}$$

where t_0 is the delay between the TDC start signal (which also triggers ejection from the MRTOF-MS preparation trap) and the actual ejection from the MRTOF-MS preparation trap. Using an oscilloscope, the delay between the trap ejection trigger and the actual trap ejection was measured to be ≈40 ns with a rise time of ≈10 ns, leading to the adoption of $t_0 = 45(5)$ ns in the analysis. The term ρ is the mass ratio evaluated from the TOF ratio, introduced to allow presentation of a simple datum for each mass measurement.

The times of flight, t, were determined by least-squares fitting of the spectral peaks to an exponential-Gaussian hybrid function [16,25] using the MPFIT package [26]. In cases with N simultaneous isobaric spectral peaks, the fitting function was a sum of N exponential-Gaussian hybrid functions each having the same width and exponential decay rate. The width and exponential decay rate were determined by scaling from the optimal fit parameters found for the drift reference ion in each measurement: $^{133}Cs^+$ ions in the first run and $^{138}BaF^+$ ions in the second run.

In the first run the gas cell was operated at cryogenic temperature, $T_{GC} \approx 70$ K. Using a beam energy of 4.825 MeV/nucleon, the $4n$ and $3n$ evaporation channel products $^{205,206}Fr^+$, as well as the $p3n$, $p2n$, $2p2n$, $2pn$, and $3pn$ evaporation channel products $^{205,206}Rn^+$, $^{205,206}At^+$, and $^{205}Po^+$ were simultaneously observed at $n = 148$ laps, as shown in Fig. 2(a). At $n = 147$ laps only the $^{205,206}Fr^+$ peaks were observed, casting some doubt on the identifications of $^{205,206}Rn^+$, $^{205,206}At^+$, and $^{205}Po^+$.

In the second run the gas cell was initially operated at $T_{GC} \approx 310$ K. Using a beam energy of 5.16 MeV/nucleon the $5n$ and $4n$ evaporation channel products $^{204,205}Fr^+$ with some evidence of $p4n$, $p3n$, $2p2n$, and $2p3n$ evaporation channel products $^{204,205}Rn^+$ and $^{204,205}At^+$ were observed at $n \in [223,226]$ laps. The gas cell was then chilled to $T_{GC} \approx 273$ K, after which the $p4n$, $p3n$, $2p2n$, $2p3n$, $3p2n$, $3pn$, and $4p$ evaporation channel products $^{204,205}Rn^+$, $^{204,205}At^+$, $^{204,205}Po^+$, and $^{205}Bi^+$ could be clearly identified at $n = 223$ laps and $n = 224$ laps, as shown in Figs. 2(b) and 2(c). These observations of so many evaporation channel products bolster confidence in the identifications assigned in the first run. Furthermore, to exclude the possibility that the lower-Z isotopes were decay products, after the $n = 223$ laps measurement the beam was stopped and a complete cessation of ion detection in the MRTOF-MS was observed almost immediately.

Since the atomic mass of ^{205}Fr was previously measured by Penning trap mass spectroscopy [27] to a higher precision than the present measurements, it was chosen as the mass reference for the present measurements to exclude possible systematic effects from a distant reference, such as that associated with uncertainty in the t_0 term of Eq. (2). However, as the rates of online ions were in all cases $\lesssim 1$ s^{-1}, ions from the offline ion source were used to perform drift correction and determine the proper fitting parameters as mentioned above.

Many isotopes in the measured region are known to have long-lived isomeric states, which in all cases are beyond the present ability of the MRTOF-MS to resolve. Unfortunately, the silicon PIN diodes used for α-decay measurements also had very low resolution (FWHM ∼ 200 keV) and could also not be used to determine the isomeric composition of the incoming evaporation products. However, in the first run a 1-ns TOF difference would represent ∼24 keV/c^2 in mass difference while in the second run it would represent ∼35 keV/c^2 in mass difference. As the FWHM of the spectral peaks was 30–40 ns, despite the inability of the MRTOF-MS to separate the isomeric states from the ground states, the presence of an admixture of isomer and ground state would produce a noticeable peak broadening.

As can be seen in Fig. 2, using widths and decay constants scaled from the drift reference produces visibly good fits, with reduced $\chi^2 \sim 1$. The exception is $^{206}Fr^+$, which exhibits an excess of counts in the tail. It is possible that this could be evidence for an admixture of the second isomeric state at 740(40) keV [28], which is at the edge of our ability to resolve. Despite the naive assumption that if the compound nucleus is initially given sufficient angular momentum the isomeric yield

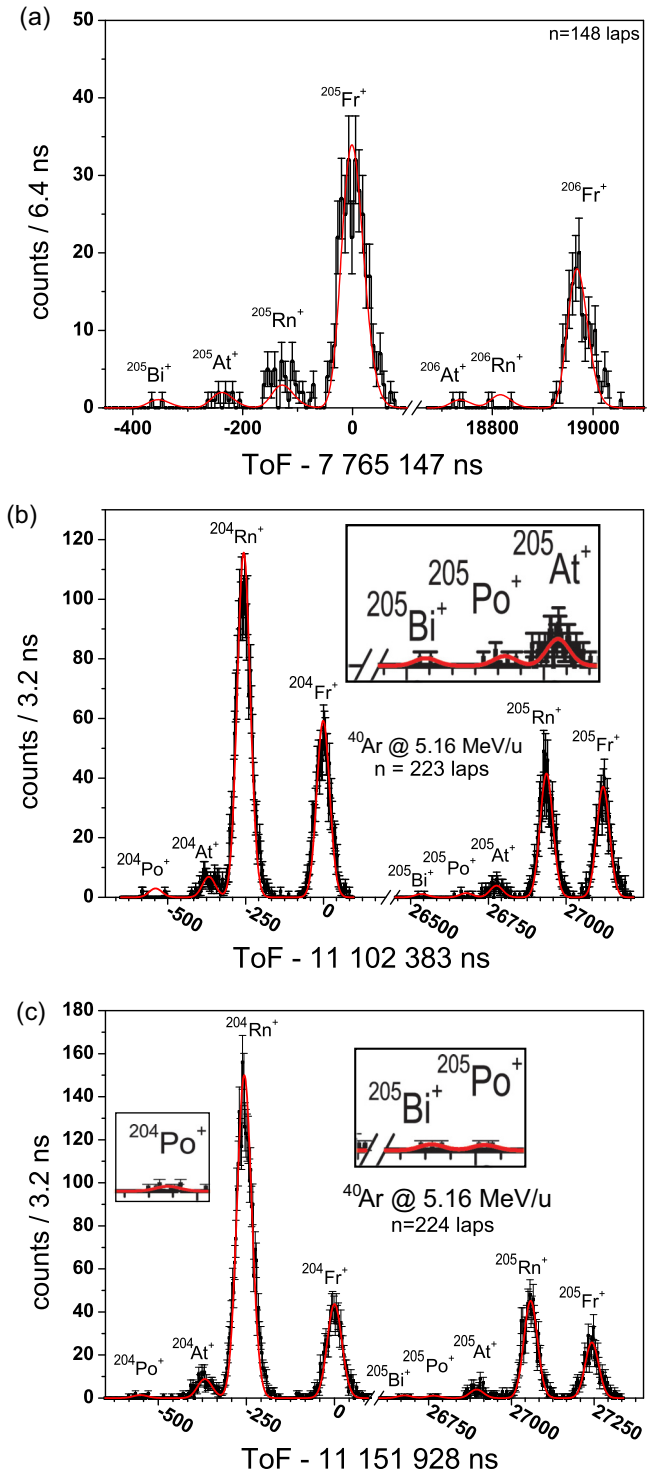

FIG. 2. Time-of-flight spectra observed using ^{169}Tm(^{40}Ar, X) reaction at (a) 4.825 MeV/nucleon and (b, c) 5.16 MeV/nucleon. Ions made (a) $n = 148$ laps, (b) $n = 223$ laps, and (c) $n = 224$ laps in the MRTOF-MS. The (a) $A/q = 205$ and $A/q = 206$ and the (b, c) $A/q = 204$ and $A/q = 205$ spectral peaks were observed simultaneously in single spectra. See text for details.

ratio should scale as $Y_m/Y_g \sim (2J_m + 1)/(2J_g + 1)$, where J_m and J_g are the spin of the isomeric and ground state, respectively [29], in all cases other than ^{206}Fr$^+$, based on the fitting quality, it is reasonable to conclude that only one highly dominant state is observed for each isotope.

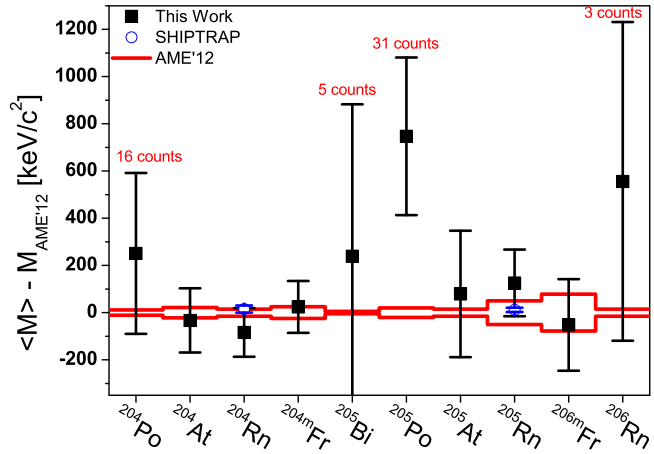

FIG. 3. Deviation of each isotope's measured mass from literature values. Error bars for this work have been scaled by the Birge ratio, when available, and include 75 keV/c^2 systematic uncertainty.

The results of our measurements are shown in Table I. The weighted average results for each isotope are given in Table II and the deviations from literature values are shown in Fig. 3. The weighted average data are generally in agreement with Atomic Mass Evaluation 2012 (AME2012) values and more recent Penning trap data for $^{204–206}$Rn [30]. In 7 of the 11 data the deviation from previous literature is less than $1 - \sigma$.

It is worthwhile to remark on the four cases where the Birge ratio–adjusted deviation from established literature values exceeded $1 - \sigma$. The first two cases, ^{204,206}Fr, are each in better agreement with their first long-lived isomeric states, at 51(4) and 190(40) keV [28], respectively, than with their ground states. Based on the aforementioned isomeric ratio expectations, this is not unreasonable.

The third case is ^{205}Po, which was identified with 31 detected ions across four measurements. The weighted average deviates from the AME2012 value by 718(258) keV. This may be a statistical anomaly, as the data are sparse, but the Birge ratio of 0.8 indicates the scattering of the data is within statistical expectations. Alternatively, there is known to be a $J^\pi = 19/2^+$ isomeric state at 1.46 MeV with $T_{1/2} = 57.4$ ms [31]. While the TOF difference between the ground state and isomer in this case is 1 FWHM, making it technically resolvable, the low statistics make separately fitting the ground state and isomeric state infeasible. The measured mass being approximately halfway between the ground state and this isomer could indicate a 1:1 mixture.

The fourth case is ^{204}Rn, which is observed to be 84(31) keV below the AME2012 values as well as previous Penning trap values. This is not likely to be a mere statistical anomaly, as the five measurements are in good agreement with each other. Nor is it likely to be evidence of isomerism, as this is an even-even nucleus. Because the historical rate of known Penning trap measurement errors is exceedingly low, we are led to believe that in this measurement the experimental spectral peak shape was not perfectly reproduced by our exponential-Gaussian hybrid function, leading to a systematic uncertainty of 75 keV/c^2 ($\delta m/m \approx 4 \times 10^{-7}$) in this work.

TABLE I. Measured data based on $^{205}Fr^{+}$ mass references. Mass data were determined using the AME2012 value for the mass of ^{205}Fr. N is the number of detected ions, while n is the number of laps.

Species	n	ρ	Mass excess (keV/c^2)	N
^{206}Fr	147	1.004 877 7(13)	−1 371(250)	66
^{206}Fr	148	1.004 879 49(61)	−1 043(120)	133
^{204}Fr	223	0.995 132 0(12)	621(242)	58
^{204}Fr	223	0.995 132 32(73)	684(140)	124
^{204}Fr	223	0.995 131 2(16)	458(307)	30
^{204}Fr	223	0.995 132 40(22)	696(42)	936
^{204}Fr	224	0.995 133 01(41)	814(79)	316
^{204}Fr	224	0.995 132 07(25)	634(48)	687
^{204}Fr	225	0.995 136 4(38)	1 462(728)	20
^{204}Fr	226	0.995 131 92(30)	605(58)	576
^{204}Fr	226	0.995 132 55(38)	724(74)	562
^{206}Rn	148	1.004 840 0(30)	−8 565(600)	3
^{205}Rn	148	0.999 967 6(16)	−7 502(320)	40
^{205}Rn	223	0.999 961 3(27)	−8 687(518)	4
^{205}Rn	223	0.999 967 16(23)	−7 579(45)	669
^{205}Rn	224	0.999 971,5(21)	−6 749(411)	7
^{205}Rn	224	0.999 966 90(24)	−7 627(47)	711
^{205}Rn	225	0.999 966 6(14)	−7 688(272)	76
^{205}Rn	226	0.999 973 9(15)	−6 279(300)	14
^{205}Rn	226	0.999 968 7(22)	−7 284(425)	7
^{204}Rn	223	0.995 086 59(19)	−8 052(38)	1790
^{204}Rn	224	0.995 086 48(21)	−8 073(42)	2323
^{204}Rn	225	0.995 085 5(13)	−8 245(253)	287
^{204}Rn	226	0.995 083 2(16)	−8 707(312)	20
^{204}Rn	226	0.995 087 2(14)	−7 934(278)	89
^{206}At	148	1.004 819(11)	−12 497(2150)	3
^{205}At	148	0.999 939 4(22)	−12 898(420)	11
^{205}At	223	0.999 938 27(66)	−13 090(127)	64
^{205}At	224	0.999 937 9(32)	−13 163(622)	2
^{205}At	224	0.999 937 78(61)	−13 188(118)	73
^{205}At	225	0.999 937 3(16)	−13 282(313)	26
^{205}At	226	0.999 942 9(10)	−12 208(193)	34
^{205}At	226	0.999 944 6(11)	−11 886(225)	39
^{204}At	223	0.995 066 9(34)	−11 851(656)	3
^{204}At	223	0.995 063 3(30)	−12 501(580)	5
^{204}At	226	0.995 066 8(17)	−11 824(331)	21
^{204}At	226	0.995 063 1(15)	−12 534(303)	92
^{204}At	223	0.995 066 56(50)	−11 877(96)	126
^{204}At	224	0.995 066 51(40)	−11 886(78)	160
^{204}At	225	0.995 066 8(16)	−11 839(313)	38
^{205}Po	148	0.999 910(10)	−18 567(2050)	2
^{205}Po	223	0.999 920 9(23)	−16 422(451)	5
^{205}Po	224	0.999 914 6(50)	−17 613(973)	3
^{205}Po	225	0.999 918 6(17)	−16 848(334)	23
^{204}Po	223	0.995 035 8(13)	−17 749(253)	4
^{204}Po	224	0.995 033 7(18)	−18 154(356)	9
^{204}Po	224	0.995 029 5(21)	−18 962(418)	4
^{205}Bi	223	0.999 895 1(56)	−21 347(1074)	2
^{205}Bi	224	0.999 898 9(35)	−20 623(670)	3

TABLE II. Weighted average data from Table I. To each datum a 75 keV/c^2 systematic uncertainty should be added to account for possible effects from imperfect peak fitting function. The deviation from literature value was calculated as $\Delta m = m_{\mathrm{MRTOF}} - m_{\mathrm{AME'12}}$. BR is the Birge ratio, by which the uncertainty should be scaled; N/A indicates there were insufficient data to calculate a Birge ratio.

Species	ρ	Mass excess (keV/c^2)	Δm (keV/c^2)	BR
^{206m}Fr[a]	1.004 879 17(55)	−1 104(107)	−52(119)	N/A
^{204m}Fr[b]	0.995 132 31(13)	679(24)	21(35)	1.11
^{206}Rn	1.004 840 0(30)	−8 565(600)	551(600)	N/A
^{205}Rn	0.999 967 14(17)	−7 584(32)	126(59)	2.1
^{204}Rn	0.995 086 51(14)	−8 067(28)	−84(31)	1.0
^{206}At	1.004 819(11)	−12 497(2150)	−69(2150)	N/A
^{205}At	0.999 939 33(37)	−12 893(71)	77(72)	2.68
^{204}At	0.995 066 40(30)	−11 908(57)	−33(61)	1.0
^{205}Po	0.999 918 9(13)	−16 791(257)	718(258)	0.8
^{204}Po	0.995 034 00(97)	−18 095(185)	246(185)	1.4
^{205}Bi	0.999 897 8(30)	−20 826(569)	238(569)	N/A

[a]May be ^{206g}Fr, with deviation from AME2012 of $\Delta m = 138(112)$ keV.

[b]May be ^{204g}Fr, with deviation from AME2012 of $\Delta m = 72(35)$ keV.

In summary, we were able to perform mass measurements on 11 nuclei in three isobaric chains during two data runs. The results of the mass evaluations are generally in agreement with AME2012 values, with the exceptions of ^{204}Rn and ^{205}Po. In the cases of ^{205}Bi, ^{204}Po, and ^{206}Rn we were able to make identifications with $N < 20$ ions. In demonstrating that the MRTOF-MS can simultaneously measure multiple isobar chains, providing precision mass measurements for higher-yield species and allowing identification of even very-low-yield species, we make the first strides toward changing the paradigm for identification of SHEs. In the near future, the device will be applied to measurements of isotopes of Md, No, Lr, Rf, and Db produced by cold-fusion reactions before being applied to hot-fusion reaction products where combined decay and mass spectroscopy will be able to enhance the veracity of new element claims. In the long term, the device will prove instrumental in identification of new SHEs. As the MRTOF-MS is, apart from a storage ring, the only method presently capable to perform precise mass measurements of multiple isobar chains simultaneously, it will also allow us to undertake an extremely efficient mass measurement campaign at the RIKEN in-flight fission and fragmentation facility as well.

We wish to express gratitude to the Nishina Center for Accelerator Research and the Center for Nuclear Science at Tokyo University for their support of online measurements. We also wish to thank S. Naimi for fruitful discussions of data analysis. I. M. acknowledges financial support provided by the RIKEN International Program Associate program. This work was supported by the Japan Society for the Promotion of Science KAKENHI (Grants No. 2200823, No. 24224008, No. 24740142, No. 15H02096, and No. 15K05116).

[1] G. I. Seaborg, Contemp. Phys. **28**, 33 (1987).
[2] R. C. Barber, P. J. Karol, H. Nakahara, E. Vardaci, and E. W. Vogt, Pure Appl. Chem. **83**, 1485 (2011).
[3] J. V. Kratz, M. Schädel, and H. W. Gäggeler, Phys. Rev. C **88**, 054615 (2013).
[4] A. V. Karpov, V. I. Zagrebaev, Y. Martinez Palenzuela, L. Felipe Ruiz, and Walter Greiner, Int. J. Mod. Phys. E **21**, 1250013 (2012).
[5] W. Loveland, K. E. Gregorich, J. B. Patin, D. Peterson, C. Rouki, P. M. Zielinski, and K. Aleklett, Phys. Rev. C **66**, 044617 (2002).
[6] D. Kaji, K. Morimoto, N. Sato, A. Yoneda, and K. Morita, Nucl. Instrum. Methods Phys. Res. Sect. B **317**, 311 (2013).
[7] G. Münzenberg, W. Faust, S. Hofmann, P. Armbruster, K. Güttner, and H. Ewald, Nucl. Instrum. Methods **161**, 65 (1979).
[8] W. R. Plaß, T. Dickel, and C. Scheidenberger, Int. J. Mass Spectrom. **349-350**, 134 (2013).
[9] H. Wollnik and M. Przewloka, Int. J. Mass Spectrom. Ion Processes **96**, 267 (1990).
[10] R. N. Wolf, F. Wienholtz, D. Atanasov, D. Beck, K. Blaum, Ch. Borgmann, F. Herfurth, M. Kowalska, S. Kreim, Yu. A. Litvinov, D. Lunney, V. Manea, D. Neidherr, M. Rosenbusch, L. Schweikhard, J. Stanja, and K. Zuber, Int. J. Mass Spectrom. **349-350**, 123 (2013).
[11] T. Dickel, W. R. Plaß, S. Ayet San Andres, J. Ebert, H. Geissel, E. Haettner, C. Hornung, I. Miskun, S. Pietri, S. Purushothaman, M. P. Reiter, A. K. Rink, C. Scheidenberger, H. Weick, P. Dendooven, M. Diwisch, F. Greiner, F. Heiße, R. Knöbel, W. Lippert, I. D. Moore, I. Pohjalainen, A. Prochazka, M. Ranjan, M. Takechi, J. S. Winfield, and X. Xu, Phys. Lett. B **744**, 137 (2015).
[12] F. Wienholtz, D. Beck, K. Blaum, Ch. Borgmann, M. Breitenfeldt, R. B. Cakirli, S. George, F. Herfurth, J. D. Holt, M. Kowalska, S. Kreim, D. Lunney, V. Manea, J. Menendez, D. Neidherr, M. Rosenbusch, L. Schweikhard, A. Schwenk, J. Simonis, J. Stanja, R. N. Wolf, and K. Zuber, Nature (London) **498**, 346 (2013).
[13] Y. Ito, P. Schury, M. Wada, S. Naimi, T. Sonoda, H. Mita, F. Arai, A. Takamine, K. Okada, A. Ozawa, and H. Wollnik, Phys. Rev. C **88**, 011306(R) (2013).
[14] Y. Ishida, M. Wada, and H. Wollnik, Nucl. Instrum. Methods Phys. Res. Sect. B **241**, 983 (2005).
[15] R. N. Wolf, D. Atanasov, K. Blaum, S. Kreim, D. Lunney, V. Manea, M. Rosenbusch, L. Schweikhard, A. Welker, F. Wienholtz, and K. Zuber, Nucl. Instrum. Methods Phys. Res. Sect. B **376**, 275 (2016).
[16] P. Schury, M. Wada, Y. Ito, F. Arai, S. Naimi, T. Sonoda, H. Wollnik, V. A. Shchepunov, C. Smorra, and C. Yuan, Nucl. Instrum. Methods Phys. Res. Sect. B **335**, 39 (2014).
[17] P. Schury *et al.*, Nucl. Instrum. Methods Phys. Res. **376**, 425 (2016).
[18] D. Kaji and K. Morimoto, Nucl. Instrum. Methods Phys. Res. Sect. A **792**, 11 (2015).
[19] F. Arai, Y. Ito, M. Wada, P. Schury, T. Sonoda, and H. Mita, Int. J. Mass Spectrom. **362**, 56 (2014).
[20] Y. Ito, P. Schury, M. Wada, S. Naimi, C. Smorra, T. Sonoda, H. Mita, A. Takamine, K. Okada, A. Ozawa, and H. Wollnik, Nucl. Instrum. Methods Phys. Res. Sect. B **317**, 544 (2013).
[21] N. E. Bradbury and R. A. Nielsen, Phys. Rev. **49**, 388 (1936).
[22] http://www.fastcomtec.com/fwww/datashee/photon/mcs6.pdf
[23] P. Schury, Y. Ito, M. Wada, and H. Wollnik, Int. J. Mass Spectrom. **359**, 19 (2014).
[24] M. Wada, P. Schury, Y. Ito, and H. Wollnik, Japanese Patent No. 2016-037679 (29th February 2016).
[25] K. Lan and J. W. Jorgenson, J. Chromatogr. A **915**, 1 (2001).
[26] C. B. Markwardt, Astronomical Data Analysis Software and Systems XVIII, **411**, 251 (2009).
[27] C. Weber, G. Audi, D. Beck, K. Blaum, G. Bollen, F. Herfurth, A. Kellerbauer, H. J. Kluge, D. Lunney, and S. Schwarz, Nucl. Phys. A **803**, 1 (2008).
[28] Georges Audi, Ming Wang, A. H. Wapstra, F. G. Kondov, M. MacCormick, X. Xu, and B. Pfeiffer, Chin. Physics C **36**, 1287 (2012).
[29] A. A. Kulko, N. A. Demekhina, R. Kalpakchieva, N. N. Kolesnikov, V. G. Lukashik, Yu. E. Penionzhkevich, D. N. Rassadov, and N. K. Skobelev, J. Phys. G: Nucl. Part. Phys. **34**, 2297 (2007).
[30] C. Droese, D. Ackermann, L. L. Andersson, K. Blaum, M. Block, M. Dworschak, M. Eibach, S. Eliseev, U. Forsberg, E. Haettner, F. Herfurth, F. P. Heßberger, S. Hofmann, J. Ketelaer, G. Marx, E. Minaya Ramirez, D. Nesterenko, Yu. N. Novikov, W. R. Plaß, D. Rodríguez, D. Rudolph, C. Scheidenberger, L. Schweikhard, S. Stolze, P. G. Thirolf, and C. Weber, Eur. Phys. J. A **49**, 13 (2013).
[31] F. G. Kondev, Nucl. Data Sheets **101**, 521 (2004).